Scientific Research Publishing

Journal of High Energy Physics, Gravitation and Cosmology, 2023, 9, 60-82
https://www.scirp.org/journal/jhepgc
ISSN Online: 2380-4335
ISSN Print: 2380-4327

The Origin of Cosmic Structures Part 5—Resolution of the Hubble Tension Problem

J. C. Botke

Nogales, Arizona, USA
Email: jcbotke(at)gmail.com

How to cite this paper: Botke, J.C. (2023) The Origin of Cosmic Structures Part 5—Resolution of the Hubble Tension Problem. *Journal of High Energy Physics, Gravitation and Cosmology*, **9**, 60-82.
https://doi.org/10.4236/jhepgc.2023.91007

Received: October 11, 2022
Accepted: January 9, 2023
Published: January 12, 2023

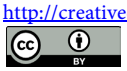

Abstract

The two principal contributors to the Hubble tension problem are the predictions of the baryonic acoustic oscillation model and the H_0 parameter fit of the "Tip of the Red Giant Branch" collaboration. In this paper, we show that the former is neither necessary nor possible and that the latter yields a value in agreement with the supernovae results when adjustments are made for errors in the peculiar velocity model used to isolate the recession velocities of galaxies. We also make comparisons between the predictions of our new model of cosmology and the curve fits of the standard model. For values of redshift ≤ 1 we find that, with a Hubble constant of $H_0 = 73$, the two agree almost exactly. We resolve the Hubble constant problem and validate the new model predictions for small redshifts.

Keywords

Hubble Tension, Expansion of the Universe, Time-Varying Curvature, Luminosity Distance

1. Introduction

One of the major problems of cosmology dating back to its beginnings in the 1930s has been to determine the value of the Hubble constant. The tension arises because the various methods applied to determine its value have yielded different values of what, in the end, must be a single number. The various determinations can be broadly separated into those involving measurements of sources with redshifts less than 6 or so and those known as cosmological determinations that argue that the CMB anisotropies are a consequence of baryonic acoustic oscillations acting on the CMB at the time of recombination when the redshift was greater than 1000. In between, the universe was filled with a neutral gas that

emitted no radiation and with no radiation, there is now nothing to observe.

What is known as the Hubble tension problem is that the cosmological determinations return a consensus value of about 67 $km^{-1}\cdot Mpc^{-1}$ whereas the moderate redshift methods are converging on a value of 73. (Henceforth, as is commonly done, we will omit the units when quoting Hubble values.) In between, the "Tip of the Red Giant Branch" (TRGB) collaboration, which covers the redshift range $z \le 0.007$, reports a value of about 69.

In this paper, we resolve the tension problem and conclude that the correct value is about 73. The bases of this determination are first, that the baryon acoustic oscillation (BAO) model upon which the cosmological value is based is simply wrong, and second, that the TRGB group determination is based on too small a sample set. When the entire set of TRGB data points is included in the analysis and a proper account of galactic peculiar velocities is taken, the TRGB data return a Hubble value of about 73 in agreement with the other determinations.

We will begin with a review of the relevant equations for both our new model of cosmology and the FRW model and then compare both with the relevant data. What we will show is that our new model's predictions are in excellent agreement with the data.

2. New Model Equations

Our new model of cosmology is based on a metric in which the curvature varies with time,

$$\begin{aligned} ds^2 = &\left(-1 + \frac{r^2 h(ct,r)^2}{a(ct)^2}\left(1 - k(ct) r^2\right)\right)(c\mathrm{d}t)^2 \\ &+ 2h(ct,r)(c\mathrm{d}t) r\mathrm{d}r + a^2(ct)\left(\frac{\mathrm{d}r^2}{1-k(ct)r^2} + r^2 \mathrm{d}\Omega^2\right). \end{aligned} \tag{2-1}$$

In [1], we explain why the scaling is given by the solution of Einstein's equations in the limit that $r \to 0$. With the above metric, the equations in that limit have an exact solution given by

$$a(ct) = a_0 \mathrm{e}^{-c_1}\left(\frac{ct}{ct_0}\right)^{\gamma_*} \mathrm{e}^{\frac{ct}{ct_0}c_1} \tag{2-2}$$

where γ_* and c_1 are constants. The former was fixed by the energy density of the CMB at the time of nucleosynthesis and has the value $\gamma_* = 1/2$. The latter is related to the Hubble constant by

$$c_1 = t_0 H_0 - \gamma_* \tag{2-3}$$

and always has a value close to 1/2. For example, with $H_0 = 73$, $c_1 = 0.525$. The curvature is given by

$$k(ct) = \frac{1}{2}\gamma_h a(ct)\kappa\left(\rho_{vac} c^2(ct) + p_{vac}(ct)\right) \tag{2-4}$$

where $\gamma_h = 1/3$ and $\kappa \equiv 8\pi G/c^4$. The sum of the vacuum energy and pressure is

$$\rho c^2(ct)+p(ct)=\frac{2k_0}{\kappa a_0^2\gamma_h}\frac{(ct_0)^2}{(ct)^2} \tag{2-5}$$

and combining gives

$$k(ct)=k_0\left(\frac{ct_0}{ct}\right)^2\left(\frac{a(ct)}{a_0}\right)^2. \tag{2-6}$$

One of the constraints of our model is that the curvature must always have its maximum possible value which results in a present-day value of

$$k_0=\frac{\gamma_*^2}{4(1-\gamma_*)}\left(\frac{a_0}{ct_0}\right)^2=1.41. \tag{2-7}$$

The model predicts a present-day exponential expansion of the scaling and a time-varying curvature proportional to the sum of the vacuum energy and pressure which varies as t^{-2}. A critical point is that, in contrast to the standard model, the exponential expansion is fixed by Einstein's equations and has nothing to do with a cosmological constant nor does it depend on the matter or radiation content of the universe. It is a kinematic consequence of time-varying curvature and the presence of the vacuum energy density and pressure in the energy-momentum tensor. The notion of the universe being radiation dominated during one epoch and matter dominated in another simply does not exist in the new model. Only one evolution is possible and it is entirely a consequence of the vacuum.

With the scaling known, we can calculate the relationship between the radial coordinate and the look-back time. Consider the path of a photon emitted by a source at t_e which is later received somewhere else at t_r. For photons, $\mathrm{d}s^2=0$ and because there are no off-diagonal components linking time and the angular coordinates, from the point of view of either the source or the recipient, $\mathrm{d}\Omega=0$. The metric becomes a quadratic equation with the solution

$$c\mathrm{d}t=\frac{a(ct)\mathrm{d}r}{\sqrt{1-k(ct)r^2}}F(ct,r). \tag{2-8}$$

The function $F(ct,r)$ is defined in [1] and has the limiting value of $F(ct,0)=1$. After rearranging and substituting $\xi=t/t_0$, we have the differential equation,

$$\frac{\mathrm{d}r}{\mathrm{d}\xi}=\frac{ct_0}{a(\xi)}\frac{\sqrt{1-k(\xi)r^2}}{F(\xi,r)} \tag{2-9}$$

which can be solved using the 4th-order Runge-Kutta method.

With the functional dependence of the radial coordinate known, we can compute the various quantities of interest. First is the redshift. The derivation is probably familiar but we will need an intermediate result later so we will run through the steps. We consider a source that emits a photon at a time t_e followed by another photon at a time $t_e+\delta_e$ or equivalently, two successive wave crests of a wave. Sometime later these are received at another location at t_r and

$t_r + \delta_r$ respectively. For the 1st photon or wave crest, the coordinate distance is given by

$$r(t_r, t_e) = \int \mathrm{d}r = \int_{t_e}^{t_r} \mathrm{d}t \frac{\mathrm{d}r}{\mathrm{d}t} \tag{2-10}$$

A similar integral exists for the 2nd photon. The coordinate distances of the two are the same since we are assuming that both the source and recipient are at rest. Expanding, we have

$$\int_{t_e+\delta_e}^{t_r+\delta_r} = \int_{t_e+\delta_e}^{t_r} + \int_{t_r}^{t_r+\delta_r} = \int_{t_e}^{t_r} - \int_{t_e}^{t_e+\delta_e} + \int_{t_r}^{t_r+\delta_r} = \int_{t_e}^{t_r} . \tag{2-11}$$

The last equality, which follows from the fact that the coordinate distance is a constant, gives

$$\int_{t_e}^{t_e+\delta_e} \mathrm{d}t \frac{\mathrm{d}r}{\mathrm{d}t} = \int_{t_r}^{t_r+\delta_r} \mathrm{d}t \frac{\mathrm{d}r}{\mathrm{d}t} . \tag{2-12}$$

Assuming that the deltas are small, we find

$$\delta_r \left.\frac{\mathrm{d}r}{\mathrm{d}t}\right|_{t_r} = \delta_e \left.\frac{\mathrm{d}r}{\mathrm{d}t}\right|_{t_e} . \tag{2-13}$$

The redshift is defined by

$$1 + z \equiv \frac{\upsilon_e}{\upsilon_r} . \tag{2-14}$$

If we consider the signal to consist of successive wave crests, the change in the travel time will vary inversely with the frequency so we have

$$1 + z = \frac{\delta_r}{\delta_e} = \frac{\left.\mathrm{d}r/\mathrm{d}t\right|_{t_e}}{\left.\mathrm{d}r/\mathrm{d}t\right|_{t_r}} . \tag{2-15}$$

The redshift is often spoken of as a Doppler shift but that is not correct because nothing is moving. It wouldn't matter except that making that assumption can lead to errors.

The luminosity distance and modulus are given by

$$D_L = a_0 (1+z) r(z) \tag{2-16}$$

and

$$\mu = 5.0 \log_{10} D_L (Mpc) + 25 \tag{2-17}$$

and the angular distance by

$$D_A(z) = a_0 \left(\frac{a(z)}{a_0} \right) r(z) . \tag{2-18}$$

We next consider the proper distance between a source and the recipient of a signal. The proper distance of some object at any particular moment is just $D_P = a(t) r$ where r is the coordinate distance. What we want, however, is the proper distance to the source measured along the path of the photon. Since the proper distance for an incremental coordinate step is $a(t)\mathrm{d}r$, the total along the path is

$$D_\gamma(z) = \int a(t)\,\mathrm{d}r = \int_{t_e}^{t_r} \mathrm{d}t\, a(t)\frac{\mathrm{d}r}{\mathrm{d}t} \tag{2-19}$$

which can be evaluated numerically using the solution of Equation (2-9).

Finally, we will need the recession velocity of the source which is given by the time rate of change of the proper distance. As we did when calculating the redshift, we consider two photons emitted a short time apart.

$$l_1 = \int_{t_e}^{t_r} \mathrm{d}t\, a(t)\frac{\mathrm{d}r}{\mathrm{d}t}, \tag{2-20a}$$

$$l_2 = \int_{t_e+\delta_e}^{t_r+\delta_r} \mathrm{d}t\, a(t)\frac{\mathrm{d}r}{\mathrm{d}t}. \tag{2-20b}$$

We expand the second integral as before but this time, the distances are not equal so we end up with

$$\begin{aligned}\Delta l &= \int_{t_r}^{t_r+\delta_r} \mathrm{d}t\, a(t)\frac{\mathrm{d}r}{\mathrm{d}t} - \int_{t_e}^{t_e+\delta_e} \mathrm{d}t\, a(t)\frac{\mathrm{d}r}{\mathrm{d}t} \\ &\approx \delta_r a(t_r)\left.\frac{\mathrm{d}r}{\mathrm{d}t}\right|_{t_r} - \delta_e a(t_e)\left.\frac{\mathrm{d}r}{\mathrm{d}t}\right|_{t_e}\end{aligned} \tag{2-21}$$

We now use Equation (2-13). Because we wish to obtain the velocity at the location of the receiver, we remove the dependence on δ_e. The velocity of recession is then

$$v_{re} = \frac{\Delta l}{\delta_r} = a(t_r)\left(1-\frac{a(t_e)}{a(t_r)}\right)\left.\frac{\mathrm{d}r}{\mathrm{d}t}\right|_{t_r} = \frac{a(t_r)}{t_0}\left(1-\frac{a(t_e)}{a(t_r)}\right)\left.\frac{\mathrm{d}r}{\mathrm{d}\xi}\right|_{\xi_r}. \tag{2-22}$$

3. Standard Model Approximations

This is a convenient time to point out that some relationships often used in the standard model are not generally true and are only accurate for small redshifts. An example often seen is the statement that $a(z)/a_0 = 1/(1+z)$. After substituting, Equation (2-18) becomes the FRW formula but since the relationship between the scaling ratio and the redshift is not generally true, neither is $D_A(z) = D_L(z)/(1+z)^2$. The redshift is given by Equation (2-15) and not by the scaling ratio.

Another example is given by the Hubble law

$$v_{re} = cz = H_0 d\,. \tag{3-1}$$

In **Figure 1**, we show the actual scaling ratio from Equation (2-2) together with $(1+z)^{-1}$. The actual ratio is shown for three values of the Hubble constant, $H_0 = 70, 73, 76$ (green, red, blue) but the differences are too small to see in the figure. Comparing, we see that the formula is only accurate for redshifts less than about $z \approx 0.5$.

In **Figure 2**, we show the individual terms making up the Hubble law calculated using the above equations for the same three values of the Hubble constant.

The left-hand equality of Equation (3-1) is judged by comparing the velocity curve with the cz curve. To assess the right-hand equality, we computed the

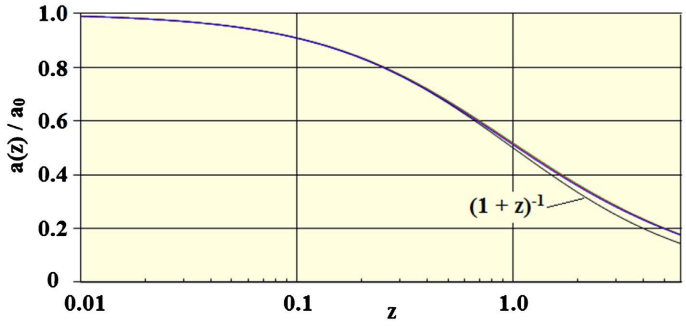

Figure 1. Comparison of actual new model scaling ratio $a(z)/a_0$ with the approximation $(1+z)^{-1}$.

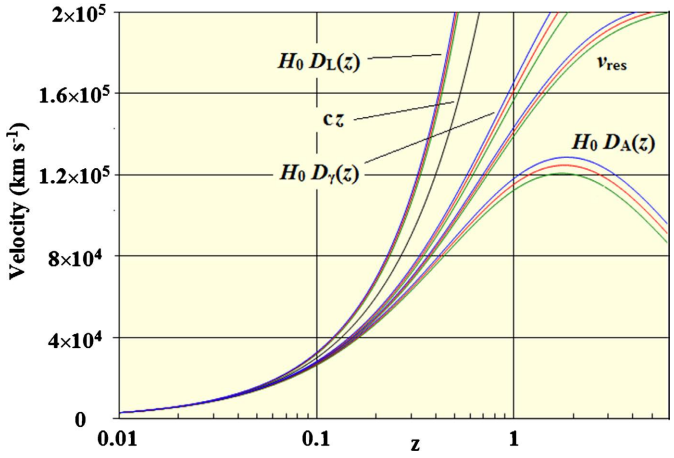

Figure 2. The terms making up the Hubble law equation.

product of the Hubble constant with first the luminosity distance, then the angular distance, and finally the proper distance. What we see is that Equation (3-1) is only accurate for redshifts in the range $z \le 0.04$ and that by $z = 0.1$, these equalities are no longer even approximately true.

4. FRW Equations

In this section, we will briefly review the FRW model equations. These equations can be found in the standard references (see e.g. [2]) but we will repeat them here so that there is no question about what we mean when we refer to a particular result.

The second of the FRW Einstein field equations can be written,

$$\frac{\mathrm{d}\bar{a}(t)}{\mathrm{d}t} = H_0\left(\frac{\Omega_m}{\bar{a}(t)} + \frac{\Omega_r}{\bar{a}^2(t)} + \Omega_\Lambda \bar{a}^2(t) + 1 - \Omega_m - \Omega_r - \Omega_\Lambda\right)^{1/2} \tag{4-1}$$

where $\bar{a}(t) \equiv a(t)/a_0$ and Ω_i are the usual densities. In terms of the dimensionless time introduced earlier, this becomes

$$\frac{\mathrm{d}\bar{a}(\xi)}{\mathrm{d}\xi} = t_0 H_0\left(\frac{\Omega_m}{\bar{a}(\xi)} + \frac{\Omega_r}{\bar{a}^2(\xi)} + \Omega_\Lambda \bar{a}^2(\xi) + 1 - \Omega_m - \Omega_r - \Omega_\Lambda\right)^{1/2} \tag{4-2}$$

We can integrate this equation with the boundary condition $\bar{a}(\xi)\big|_{\xi=1}=1$ to determine the scaling. Rearranging and integrating from some point in the past up to the present, we have

$$\frac{1}{t_0 H_0}\int_{\bar{a}(\xi)}^{1} \mathrm{d}\bar{a}'\left(\frac{\Omega_m}{\bar{a}'}+\frac{\Omega_r}{\bar{a}'^2}+\Omega_\Lambda \bar{a}'^2+1-\Omega_m-\Omega_r-\Omega_\Lambda\right)^{-1/2}=\int_{\xi}^{1}\mathrm{d}\xi'=1-\xi\,. \quad (4\text{-}3)$$

The LHS is just an ordinary integral which can be evaluated numerically for any set of densities. To determine $\bar{a}(\xi)$ for any ξ, we apply Newton's method to the function, $F(\bar{a})=\mathrm{LHS}-(1-\xi)$ so $\bar{a}_n=\bar{a}_{n-1}-F(\bar{a}_{n-1})/F'(\bar{a}_{n-1})$ where

$$F'(\bar{a}_{n-1})=\frac{-1}{t_0 H_0}\left(\frac{\Omega_m}{\bar{a}_{n-1}}+\frac{\Omega_r}{\bar{a}_{n-1}^2}+\Omega_\Lambda \bar{a}_{n-1}^2+1-\Omega_m-\Omega_r-\Omega_\Lambda\right)^{-1/2} \quad (4\text{-}4)$$

By construction, $\bar{a}(1)=1$ but in general, the solutions do not satisfy the condition that $\bar{a}(0)=0$, and in fact, there is no reason why they should given that the universe began with Plank dimension uncertainties and inflation. An alternate approach is to specify different values of the scaling and then use the equation to determine the corresponding lookback time.

In a few special cases, (4-3) can be solved exactly. For example, with $\Omega_r=0$ and $\Omega_m+\Omega_\Lambda=1$,

$$\bar{a}(\xi)=\left(\frac{1-\Omega_\Lambda}{\Omega_\Lambda}\right)^{1/3}\sinh^{2/3}\left(\sinh^{-1}\left(\sqrt{\frac{\Omega_\Lambda}{1-\Omega_\Lambda}}\right)-\frac{3t_0 H_0}{2}\sqrt{\Omega_\Lambda}(1-\xi)\right). \quad (4\text{-}5)$$

This scaling vanishes when the argument of the hyperbolic sine vanishes. With $\Omega_\Lambda=0.76$ and $H_0=74$, this happens at a value of $\xi=0.0185$ or $t=8.0\times10^{15}$ s so even though this is a solution, it obviously doesn't describe reality.

With the FRW metric, the scaling ratio approximation formula is actually true,

$$1+z=a_0/a(t)\,. \quad (4\text{-}6)$$

If we substitute this result into Equation (4-3), we obtain a formula for the lookback time in terms of the redshift,

$$1-t/t_0=\frac{1}{t_0 H_0}\int_0^z \frac{\mathrm{d}z'}{1+z}\left(\Omega_m(1+z')^3+\Omega_r(1+z')^4+\Omega_\Lambda+\Omega_k(1+z')^2\right)^{-1/2}. \quad (4\text{-}7)$$

We point out that, while this formula is commonly used, if one tries to normalize this result by integrating to $z=\infty$, we find that infinite numerical precision is required. More specifically, for any given numerical step size, there is an upper limit on z beyond which the integral becomes unstable.

Using Equation (4-6), we have

$$\mathrm{d}(1+z)=\mathrm{d}\left(\frac{a_0}{a(t)}\right)=-\frac{a_0}{a(t)}\frac{\dot{a}(t)}{a(t)}\mathrm{d}t=-(1+z)H(z)\mathrm{d}t \quad (4\text{-}8)$$

which will give us a shortcut to the comoving coordinate. Consider now a photon emitted at a time t and received later at t_0. With the FRW metric, we have

$$\chi = \int_t^{t_0} \frac{c\mathrm{d}t'}{a(t')} = \frac{c}{a_0}\int_0^z \frac{\mathrm{d}z'}{H(z')} \tag{4-8}$$

Substituting (4-6) into (4-1) results in a formula for $H(z)$ which we can then substitute into (4-8). The result is a formula for the comoving coordinate of the source as a function of the redshift. With this, we now obtain the luminosity and angular distances using the usual formulas, $D_l = a_0 S(\chi(z))(1+z)$ and $D_A = a(t)S(\chi(z)) = \frac{a_0}{1+z}S(\chi(z))$.

With the formulism complete, we can now turn to the Hubble tension problem.

5. Redshifts Greater than 0.01

In one form or another, the moderate redshift determinations are based on the use of a standard candle which is a type of source that has a known intrinsic magnitude. We will first review the type Ia supernovae results. In this method, after calibration against a local source at a known distance, Equations (2-16) and (2-17) or their FRW equivalents can be used to determine the distance. The earliest results date back to the 1990s [3]. Since that time, a huge number of observations have been reported. (See e.g. [4].) Our interest is not so much in exhaustive data fits but with the model predictions. In **Figure 3**, we show only a limited set of data points. The blue points are from [3] and the red points are from [5]. In the latter case, the 4 data points with the largest redshifts are shown explicitly but for the remainder, only the general trend is indicated with the light red band.

We find that the model predictions for the range of Hubble constants indicated are almost indistinguishable. The curves appear to lie slightly below the Riess data points but agree with the Nielsen points. As a test, we varying k_0 and γ_* by factors of 2 and found no change in the model predictions. What this means is that it either agrees with the data or doesn't because its prediction cannot be altered.

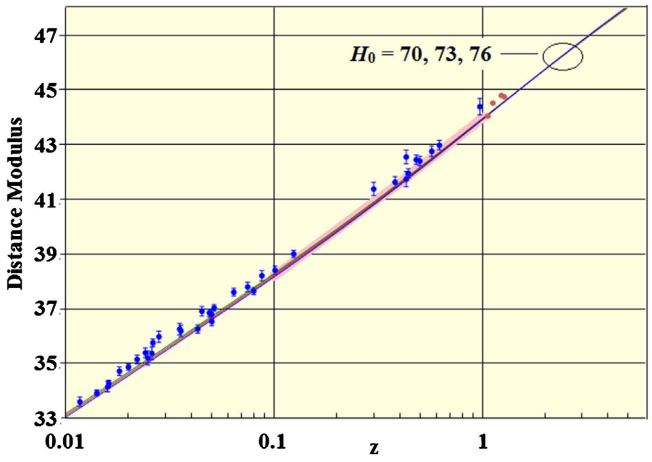

Figure 3. Luminosity distance modulus with the new model predictions for $H_0 = 70, 73, 76$.

We now compare with the FRW results. In Figure 4, we show the new model predictions for two values of the Hubble constant on the left and the FRW predictions for the same two values on the right.

We see that predictions are similar with the new model exhibiting less variation with changes in the Hubble constant. In [4], the authors report a value of $H_0 = 73.04 \pm 1.04$. For that value, the two predicted curves are identical for $z < 1.0$ as shown in Figure 5. The model predictions do begin to diverge for larger values of redshift

Since the new model prediction is the same as the FRW prediction in the range $z < 1.0$, a fit based on the new model will yield the same value of the Hubble constant as does the FRW model so this stands as a validation of the new model.

We next consider the approach known as the L-σ method which was pioneered by Melnick [6] and others. The method is based on an observed correlation between the luminosity distance of large HII regions or galaxies and the velocity distribution of the width of their Hβ emission lines. Recent results using

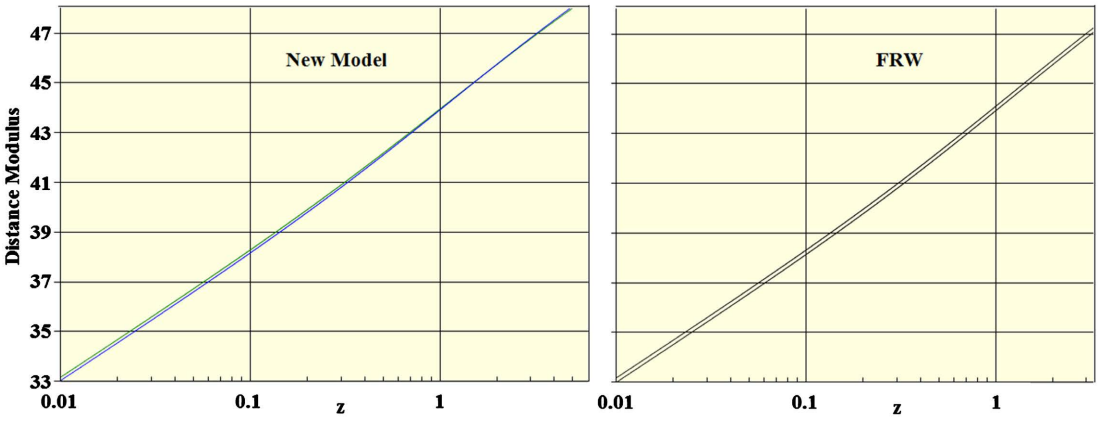

Figure 4. Model and FRW predictions for $H_0 = 70$ and $H_0 = 76$. The FRW parameters are $\Omega_m = 0.3$ and $\Omega_\Lambda = 0.7$.

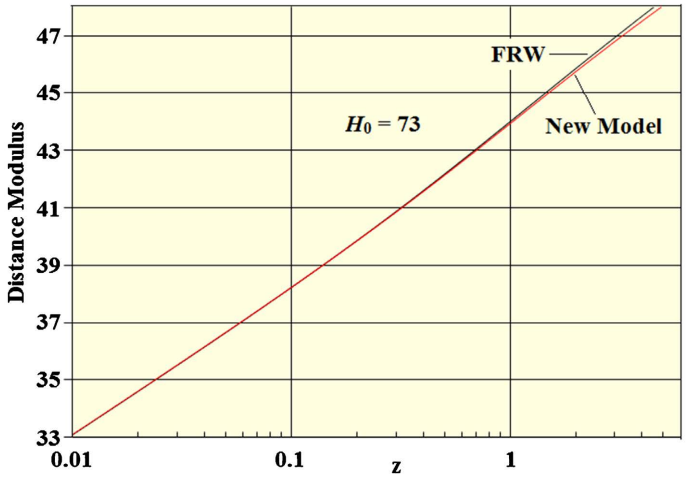

Figure 5. New model (red) and FRW (black) predictions for $H_0 = 73$.

this method are discussed in [7]. One of the advantages of this method is that it extends the redshift range beyond that achieved with the supernovae approach. The distance results[1] are shown in Figure 6. There is some scatter in the larger redshift data points but this is a new method and it is expected that the errors will be reduced as more experience is gained.

In that paper, the authors report the value $H_0 = 71.7 \pm 1.8$ which is consistent with the supernovae results. In Figure 7, we show χ^2 results calculated against the new model prediction. In the upper panel, we included just the points with redshifts less than 0.4, and in the lower panel, with redshifts greater than 0.4. In the former case, the minimum is for a value of about 75 but the standard deviation is large. With the upper points, the curve is flat so no determination is possible.

The next method is known as the megamaser method [8]. In this case, the

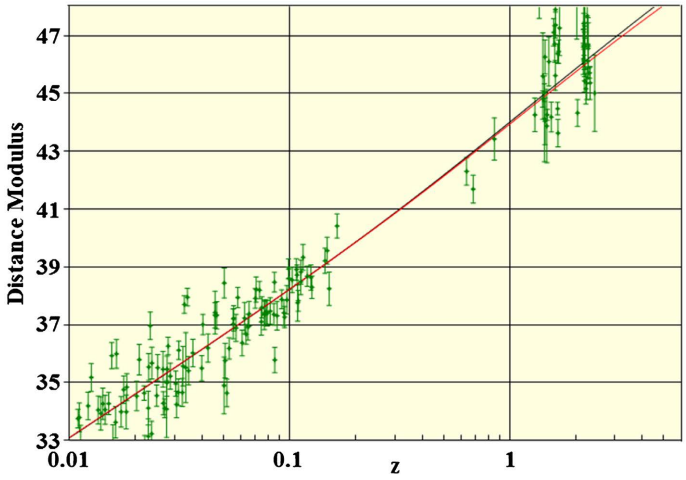

Figure 6. Distance measurements using the L-σ method. The curves are the same two curves shown in Figure 5.

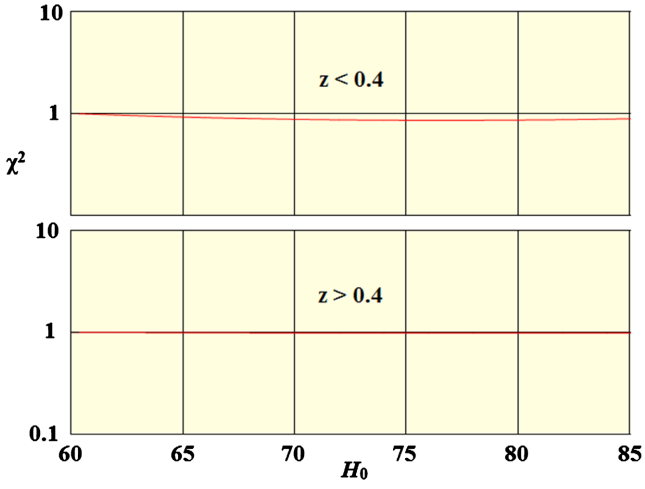

Figure 7. χ^2 against the new model prediction for the data points of Figure 6 with the cutoffs indicated.

[1]Gonzales-Moran, A.L. (2022) Private Communication.

angular distance to several galaxies was measured directly using very long baseline interferometry. This method bypasses uncertainties inherent in the previous methods because of their dependence on a chain of calibrations to resolve the distances. The results are shown in Figure 8 along with the new model predictions for the same three values of the Hubble constant.

We see that the measured distances are in very good agreement with the predictions of the new model. The Hubble constant reported in [8] is $H_0 = 73.9 \pm 3.0$ which is in agreement with the previous results. The galaxy in red is NGC 4258 which is commonly used as a calibration galaxy in other studies. The remaining galaxies have redshifts that coincide with those at the lower end of the supernovae' redshift range.

As part of this work, the velocities of the megamaser components were determined by first determining the component redshifts from the detected spectral frequency shifts and then applying the rule, $v = cz$. The recession velocities were afterward determined by averaging the component velocities. In Figure 9, we compare these recession velocities with Equation (2-22) and find a close match.

In this case, the use of $v = cz$ is justified but the galaxy at the largest redshift is approaching the limit.

6. Redshifts between 0.001 and 0.01

We will now consider the redshift range, $0.001 \le z \le 0.01$. For redshifts larger

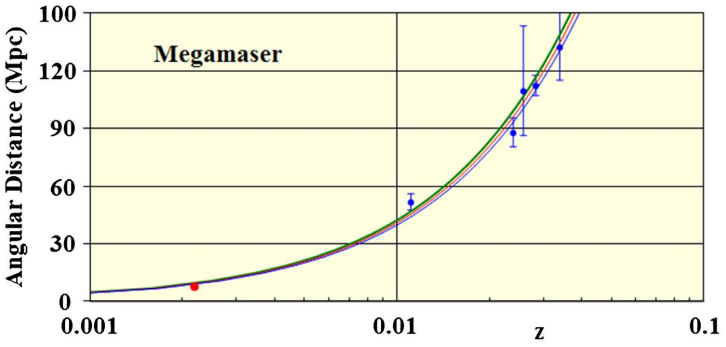

Figure 8. Megamaser angular distance results.

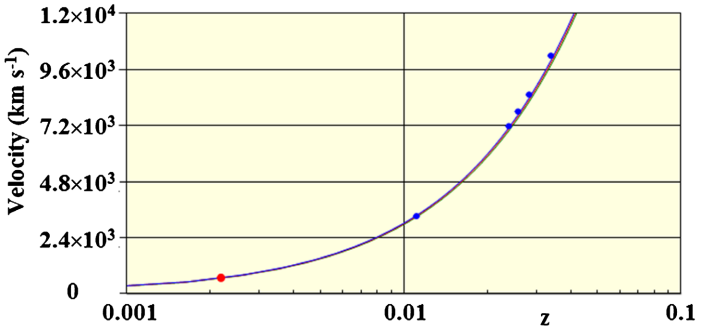

Figure 9. Megamaser recession velocities compared with the new model prediction, Equation (2-22).

than 0.01, the peculiar velocities of the galaxies are relatively small in comparison with the recession velocity so we obtain the expansion redshifts directly. For redshifts below 0.01, this is no longer the case. As we move to smaller distances, the peculiar velocities can become as large or even larger than the recession velocities and, unfortunately, observations alone cannot separate the two.

To separate the two, a statistical model has been under development for the past 2 decades that estimates the recession velocity field in a probabilistic sense, see e.g. [9]. The assumption is made that the peculiar velocities are a result of variations in the gravitational field due to the local distribution of matter (which might not be entirely true.) It is also assumed that the galaxy velocity distributions are Gaussian. The overriding issue with this approach is that it is statistical rather than deterministic and so it is inevitable that there will be errors in the velocity predictions. In what follows, we will show that for redshifts at the lower end of the range we are considering, there seems to be a systematic bias that results in an underestimation of the recession velocities for some regions of the local universe.

The results shown in the remainder of this section are based on data taken from the Extragalactic Distance Database (EDD or NED) [10]. This site also contains two implementations of the recession velocity estimation model.

As a preliminary exercise, we randomly selected a list of galaxies with *observed* redshifts in the range $0.003 \le z \le 0.01$ from the "Cosmicflows-3 Distances" database contained in the EDD. The result is shown in **Figure 10**.

The curves shown are the new model predictions; the FRW predictions are similar. For each of these galaxies, we then calculated their probabilistic recession velocity using one or the other of two tools available on the opening page of the EDD. The result is shown in **Figure 11**.

These results give us an inkling of a problem with the flow field model. If the model were perfect, all the data points would lie along a line parallel to the predicted curves. That is generally the case at the upper end of the redshift range but there is perhaps a systematic deviation for smaller redshifts. In **Figure 12**, we show two χ^2 results. The upper (red) curve was calculated with all the galaxies included and the lower curve (green) with only those with redshifts $z \ge 0.006$.

The curves are normalized by the value of the upper curve at the left boundary

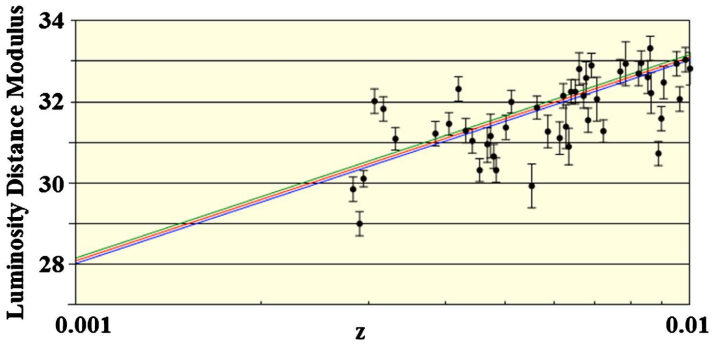

Figure 10. Randomly selected galaxies in the redshift range $0.003 \le z \le 0.01$.

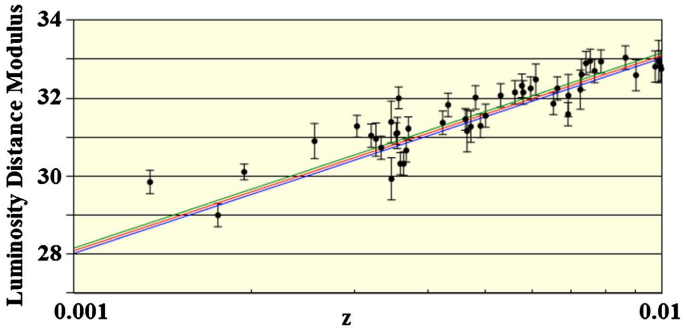

Figure 11. Galaxies from Figure 9 after correcting for peculiar velocities.

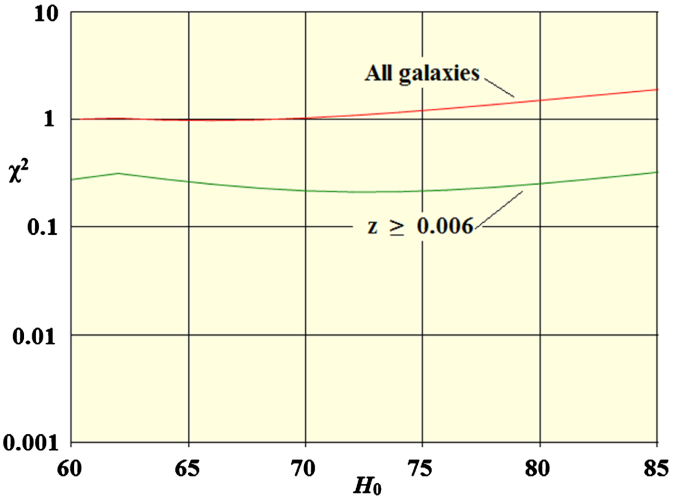

Figure 12. Normalized χ^2 curves for the galaxy distribution of Figure 10.

of the chart. We are only interested in the shape of the curves so this does not cause a problem. We immediately see that the full set of galaxies indicates a Hubble constant in the low 60 s but when we limit the list to those with $z \geq 0.006$, we find a value of $H_0 \approx 73$. We could include additional galaxies (there are more than 17,000 entries in the database) but we would not learn much more than we now know. The flow field velocity model seems to give reasonable results for $z \geq 0.006$ but for smaller redshifts, its accuracy appears to deteriorate.

We will next discuss TRGB results which constitute the midrange portion of the Hubble tension problem. Refer to e.g. [11] for a review of the method. The method is based on the use of a specific group of red giant stars as a standard candle and as far as determining distances, the method works well. The group then goes on to predict the Hubble constant and there they run into problems. Their result is $H_0 = 69.8 \pm 0.6(\text{stat}) \pm 1.6(\text{sys})$. The problem with this determination is that it is based on a total of only 18 galaxies which is an extremely small fraction of the total of 558 galaxies in the TRGB database. We first show in Figure 13 our results for the list of galaxies used to determine the Hubble constant in [11] that lie within the redshift range we have been discussing. The galaxies are plotted according to their observed redshifts in green and, after adjustment,

in blue.

We see the same problem we encountered earlier, namely that the flow field values do not line up along a line parallel to the predictions. In this case, we obtained the distances and redshifts using values from the CMBs/TRGB database together with the flow velocity tools but for some reason, our redshift values do not agree with those listed in [11]. The differences are shown in Figure 14.

In Figure 15, we show the χ^2 results. Our determination is shown in green

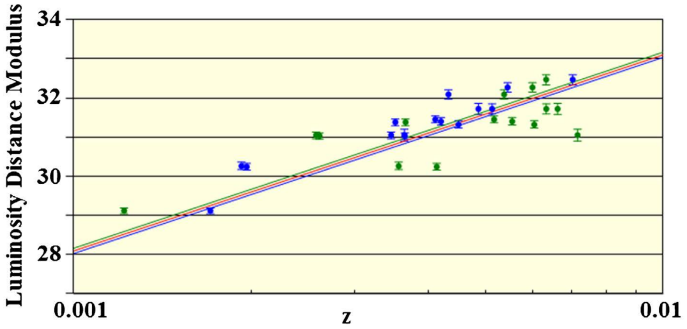

Figure 13. Distribution of the galaxies used in [11] for their determination of the Hubble constant. The galaxy positions shown in green were plotted using the observed redshift and those shown in blue were plotted using the flow field model redshifts.

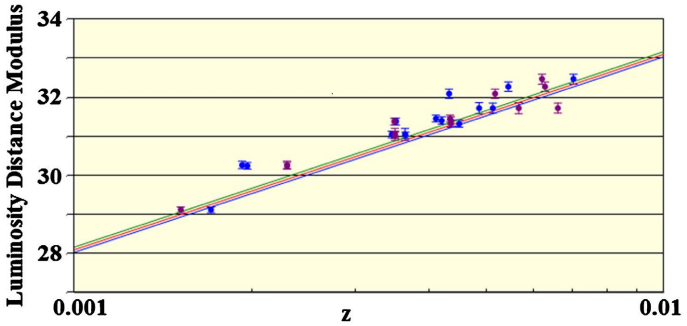

Figure 14. Our determinations of the corrected redshifts for the selected galaxies are shown in blue and those reported in [11] are shown in red.

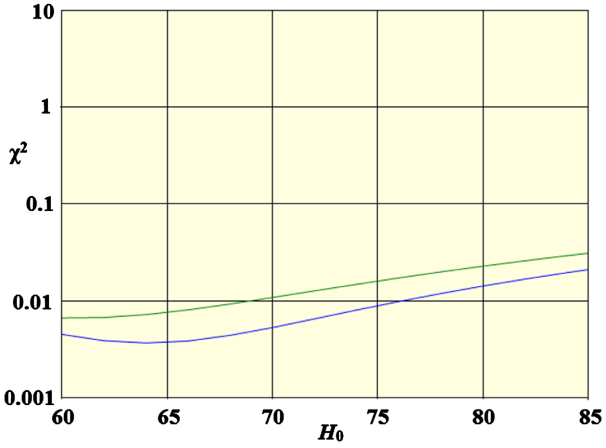

Figure 15. χ^2 results for the two data sets shown in Figure 14. Our result is shown in green and the result obtain using the values from [11] is shown in blue.

and the result using the values from [11] is shown in blue.

We see that both data sets from Figure 14 indicate a Hubble constant well below 70. From such a small sample of galaxies, it isn't possible to firmly rule out the value of the Hubble constant reported in [11] so the next step is to include the entire list of TRGB galaxies. We first listed all the 558 entries in the CMDs/TRGB database. Next, because the TRGB database does not contain either the redshift or the observed velocity, we linked the TRGB database to both the LEDA and the Kourkchi-Tully (KT) redshift catalogs to determine the observed velocities ("v3k"). We then restricted the list to those with *observed* redshifts in the range $z \geq 0.001$. Finally, by hand, we added the 4 galaxies used in [11] that have blank distance modulus values in the TRGB database. The final count was then 291. The result is shown in Figure 16.

The next (rather tedious) task was to determine the flow field model redshifts for the entire set of galaxies. The results are shown in Figure 17.

To get an idea of the size of the flow field model corrections, in Table 1, we show the distribution of the ratio, z_{ff}/z_{obs} for the data set shown in Figure 17.

We see that the peculiar velocity can be almost 3 times as large as the recession velocity and that the most common value is about 1/2 the recession velocity which supports our earlier statement that the peculiar velocities are large for galaxies in this range of redshifts.

Referring back to Figure 17, we see that a large percentage of the points lie along the predicted curves indicating that the flow field model is working

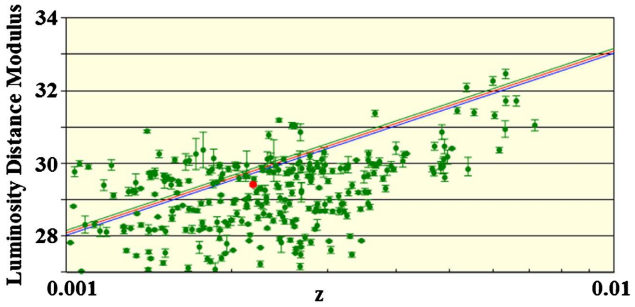

Figure 16. Galaxies from the TRGB database as described in the text. The galaxy shown in red is NGC4258 which is often used as a calibration point.

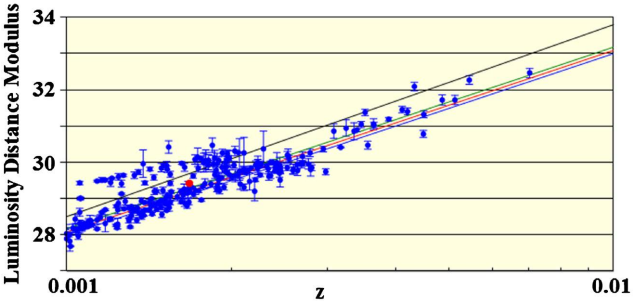

Figure 17. The set of galaxies from Figure 16 plotted using the flow field model redshifts. For comparison, we show the FRW model prediction curves instead of the new model curves. The black line is explained in the text.

reasonably well for those cases but there are also a considerable number of galaxies with recession velocities that are far too small as indicated by the points lying above the predicted curves. Remember that the points move horizontally with a change of redshift so all the points lying above the predicted curves would need to move to the right to correspond to the model predictions.

The χ^2 shown in the upper panel of Figure 18 for the full set of data points indicates a Hubble constant of $H_0 \sim 66 - 67$. To assess the importance of the outliers, we introduced a cutoff as shown in black in Figure 17. With the galaxies lying above that line removed, the χ^2 shown in the lower panel indicates a value of $H_0 = 73 - 74$. We find that the low value obtained from the full data set is solely a consequence of errors in the flow field model predictions and when allowances are made for what appear to be systematic errors, the full TRGB data set supports a value of $H_0 = 73$ in agreement with the larger redshift determinations.

Table 1. Distribution of the (flow field velocity)/(observed velocity) ratio.

Range	Count	Range	Count
2.4 - 2.8	2	0.8 - 1.0	42
2.2 - 2.4	2	0.6 - 0.8	65
2.0 - 2.2	1	0.4 - 0.6	84
1.8 - 2.0	2	0.2 - 0.4	8
1.6 - 1.8	6	0 - 0.2	0
1.4 - 1.6	6		
1.2 - 1.4	13		
1.0 - 1.2	13		

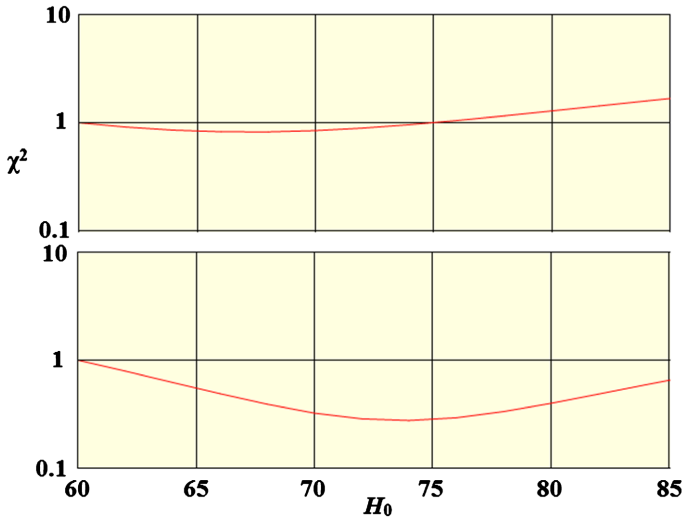

Figure 18. χ^2 results for the dataset of Figure 17. The result for the full set is shown in the upper panel and the result with the galaxies above the cutoff line removed is shown in the lower panel.

7. Baryonic Acoustic Oscillations

In this section, we will show that baryonic acoustic oscillations are neither necessary nor possible and that the phenomena that they are supposed to explain are quite natural and unavoidable consequences of our new model of cosmology. The two phenomena in question are the anisotropy of the CMB spectrum and the bump in the galactic two-point correlation function at a separation of 150 Mpc. We will first give two arguments to show that the BAO model just doesn't work and then show that the new model does account for both phenomena.

The BAO model does not make any attempt to explain the origin of either the baryonic matter of the universe or the radiation making up the CMB. Instead, those are taken as given. The model then supposes that, however the radiation came into existence, it was uniformly distributed throughout the universe and in need of some agent to create the observed anisotropies. With this premise, the BAO model is already wrong because it ignores the fact that the anisotropies could have been introduced at the time the radiation came into existence which is precisely what did happen according to our new model of nucleosynthesis. Nevertheless, we will carry on to show that the BAO idea is impossible.

The first problem is causality. We show in [1] that superclusters have the right size to account for the first peak of the CMB spectrum. Later we realized the superclusters were not responsible for the CMB as we first thought but instead, the process that created the superclusters at the time of nucleosynthesis simultaneously created the CMB complete with its anisotropies that had the same dimensions as the superclusters. The present-day sizes of the superclusters thus give us a reference dimension. At $t = t_{rec}$, the average size of a supercluster was $l_{sc}(t_{rec}) = 4.0\times10^{21}$ m and the scaling was $a(t_{rec}) = 4.0\times10^{23}$ m. The coordinate size of an average supercluster is then $r_{cs} = l_{cs}(t_{rec})/a(t_{rec}) = 0.01$ which is a value that doesn't change with time because superclusters are too large for their dimensions to evolve. In **Figure 19**, we show the coordinate path, calculated by integrating Equation (2-9), of a photon emitted at the time of nucleosynthesis from one end of a supercluster, From the figure, we find that by the time of recombination, the photon has only traveled about 10% of the dimension of the supercluster which rules out the possibility that an acoustic wave could traverse the full dimension of a supercluster in the same period. There are other comparisons we could make but they all amount to the same thing. Superclusters, and

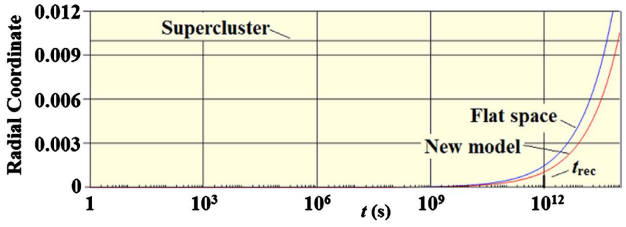

Figure 19. Radial coordinate of a photon emitted at the time of nucleosynthesis. The red curve is the new model result and the blue curve is the flat universe result. The black horizontal line $r_{SC} = 0.01$ is the constant coordinate dimension of an average supercluster.

hence the width of the first peak of the CMB spectrum, are too large to be the consequence of any causal process.

We will next consider the energy requirements. The energy density of blackbody radiation is given by $\rho_{BB} = a_{SB}T^4$ where $a_{SB} = 7.5657\times10^{-16}\ \mathrm{j\cdot m^{-3}\cdot K^{-4}}$. At present, the variance of the CMB spectrum has a peak value of $\Delta T_0 = 200\ \mu\mathrm{K}$ so

$$\frac{\Delta T_0}{T_0} = 2\times10^{-4}. \tag{7-1}$$

Earlier, at the time of recombination, the variance ratio was the same but the temperature was then $T_{rec} = 3000\ \mathrm{K}$. The energy density of the anisotropies is easily calculated,

$$\rho_{\Delta T} = a_{SB}\left(\left(T+\Delta T\right)^4 - T^4\right) \approx 4a_{SB}T^4\frac{\Delta T}{T} = 4.9\times10^{-5}\ \mathrm{j\cdot m^{-3}}. \tag{7-2}$$

Next, we assume that the expanding acoustic wave had a radius on the order of 1/2 the dimension of a supercluster so the volume was on the order of $V = 4\pi\left(l_{sc}/2\right)^2\Delta l_{sc}$. If we now assume a thickness equal to 10% of the radius, we find that $V = 1\times10^{64}\ \mathrm{m^3}$ so the total energy required is

$$E_{total} = 4.9\times10^{59}\ \mathrm{j}. \tag{7-3}$$

The BAO model assumes that this energy originated in a concentrated source whose size at the time of nucleosynthesis could not have been greater than $l_S = ct_n$. Since $t_n \approx 10^{-5}\ \mathrm{s}$, the volume of the source could not have been greater than $V_S \approx 4.2\times10^{12}\ \mathrm{m^3}$ which implies an energy density of $\rho_S = 1.2\times10^{47}\ \mathrm{j\cdot m^{-3}}$. But the total vacuum energy density at that time, which constituted the entire energy of the universe, was just $\rho_{vac} = 3.6\times10^{34}\ \mathrm{j\cdot m^{-3}}$ so the energy needed by the BAO to account for the CMB anisotropies was 10^{12} times greater than the total energy density of the universe. This is even more of a problem when one considers that the BAO model assumes that the energy results from a small perturbation on a radiation field that, at the time of nucleosynthesis, had an energy density of $\rho_{CMB} = 2.6\times10^{31}\ \mathrm{j\cdot m^{-3}}$. While this estimation is simplistic, the disparity is so large that the conclusion is unavoidable. The BAO cannot possibly account for the CMB anisotropy spectrum and it immediately follows that the BAO model cannot be used to place bounds on the Hubble constant.

We can go even further to show that no event at the time of nucleosynthesis can yield such a bound. Referring back to Equation (2-2), the Hubble constant enters the equation via the constant c_1 but at $t = t_{rec}$, the exponential has the value

$$\mathrm{e}^{\frac{ct}{ct_0}c_1} = \mathrm{e}^{1\times10^{-6}} = 1 \tag{7-4}$$

which means that the scaling is purely power-law during that epoch. The present-day Hubble constant does not become significant until the point is reached when the exponential acceleration of the expansion begins to become a factor and that didn't happen until shortly before the time of galaxy formation [1].

In the new model of cosmology, the existence of matter is a consequence of a small percentage of the vacuum energy being converted into neutron/antineutron pairs with a very small excess of neutrons. Most of the pair underwent annihilation into photons, electrons, and neutrinos with the photons eventually becoming the CMB. The CMB anisotropies were an unavoidable consequence of this process and hence the spectrum was built in at the beginning. The details are given in [12].

We now turn to the second phenomenon attributed to BAO, namely the bump in the two-point correlation function at a separation of 150 Mpc. Since the BAO are impossible on a scale necessary to account for the large-scale features in question, there must be another explanation and the explanation is obvious; it is the cosmic web.

To demonstrate that this is the case, we created a simple numerical model of the cosmic web. We started with a cubic grid in which all the edges had lengths equal to the average size of a supercluster. Then, using Gaussian statistics, we offset each edge connection point in a random direction by a random amount scaled by the known distribution of supercluster sizes shown in [1]. We then added a random number of galaxies along each adjusted edge with each galaxy given a random offset in both direction and magnitude scaled by the average width of a cosmic web filament. To minimize edge effects, we made the grid significantly larger than the maximum correlation distance of interest. We then trimmed the list of galaxies to those that lay within an assumed maximum distance of each of the reference galaxies attached to the center edge line of the grid. The average present-day size of superclusters is about 4.4×10^{24} m = 143 Mpc and, as shown in [1], the supercluster size distribution is Gaussian with a relative standard deviation of about 0.27. Since we adjusted both ends of each edge, we used a value of 0.14 when randomizing the endpoints of each edge.

We then calculated the correlation function using the formula [13],

$$1+\xi(r)=\frac{1}{N}\sum_{i=1}^{N}\frac{N_i(r)}{\overline{n}V_i(r)}. \tag{7-5}$$

In this formula, the number of reference galaxies is given by N and $\overline{n}$ is the average density of all the galaxies. $N_i(r)$ is the number of galaxies lying within a spherical shell of radius r and volume, $V_i(r)$ centered on the *ith* reference galaxy. The ratio compares the actual number in each shell with the number expected based on the average density of the galaxies. If the galaxies were distributed randomly, we would have $\xi(r)=0$.

We ran the simulation multiple times with different sets of random numbers. The number of galaxies along each leg varied randomly between 20 and 30 with a relative position variance of 0.2. In **Figure 20**, we show the results for 10 runs.

The result compares favorably with the shape of the observed correlation function shown in, for example, [14] and the peak is at the right distance.

To summarize, we have shown that the BAO model is simply wrong and neither

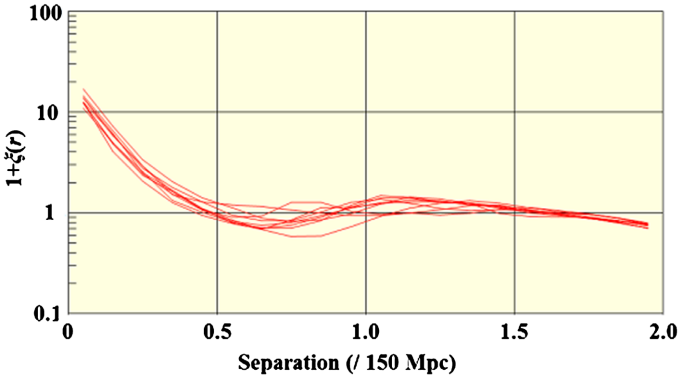

Figure 20. Randomized cubic grid model of cosmic web two-point galaxy correlation function.

is it necessary. The CMB anisotropy spectrum is an unavoidable outcome of the new model of nucleosynthesis and the two-point correlations are simply a reflection of the cosmic web.

With the elimination of the BAO model, the Hubble tension problem ceases to exist.

8. Solar System Expansion

Another approach to the Hubble problem that completely bypasses the peculiar velocity issue is based on the fact that, in addition to whatever other accelerations are at play, all structures are subject to the expansion of the universe. In some cases, such as with stars, the expansion does not result in any detectable change of dimension because the combined attractive and repulsive forces acting on the star result in an equilibrium that completely overrides the expansion. This condition does not exist, however, for more loosely bound systems such as the orbits of planets or moons. In these cases, the expansion results in a slow increase in the distances between orbiting bodies.

Measuring the rate of expansion of the planets and moons with sufficient accuracy is now feasible in many cases with the prime example being the Earth's moon. Data accumulated during the past 70 years has now fixed its annual recession rate at a value of 3.83 ± 0.009 cm·yr^{-1} [15] [16]. Calculating the portion of the recession due to the expansion is not difficult as we will show below. The problem, and it is a big one, is accurately accounting for all the other forces that act on the body in question. In the case of the Moon, tidal forces dominate and their calculation involves the motion of the oceans, continental drift, the shifting of the ice pack, the motion of Earth's core, and so on. To place a bound on the Hubble constant, all these contributions must be known with a combined error of no more than 2%.

The advantage of this approach, on the other hand, is that if all the other problems can be solved, the portion of the recession due to the expansion is directly proportional to the Hubble constant and is easy to calculate. Any distance can be written as the product of the coordinate distance multiplied by the scaling

so the Earth-Moon distance, for example, varies according to

$$R(t)=r(t)a(t)=\bar{r}(t)\frac{a(t)}{a_0}. \tag{8-1}$$

The coordinate distance $r(t)$ has no units. The variable $\bar{r}(t)=r(t)a_0$ with the units of length is the actual present-day Earth-Moon distance. The variation of the coordinate distance is a consequence of the tidal, etc., forces. To determine the portion of the recession that is a consequence of just the expansion, we hold the coordinate distance constant and find

$$R(t+\Delta t)=R(t_0)\left(1+\frac{\dot{a}(t_0)}{a(t_0)}\Delta t\right)=R(t_0)(1+H_0\Delta t). \tag{8-2}$$

Putting in numbers, with $H_0=73$ we find $v_{em}=2.84$ cm/yr.

We can just as easily calculate the change in the recession rate over time. With the coordinate distance again held constant, the velocity is given by $v_{em}(t)=R(t_0)\dot{a}(t)/a(t_0)$. The age of the Moon is on the order of 4 billion years which corresponds to a time ratio of 0.7. In Figure 21, we show the results for the same three values of H_0.

We see that the recession rate has not changed much during the lifespan of the Moon but the increasing spread between the curves shows that the rate is more sensitive to the value of H_0 at present than it was in the past. The importance of this result is that it shows that the calculated expansion does not imply some impossibility such as a requirement that the Moon be inside the Earth at some point in the past.

There are many papers to be found on the internet for those interested in following this further.

9. Conclusions

In this paper, we have shown that the BAO model is wrong so its prediction of the Hubble constant can be dismissed. We also showed that after making adjustments for errors in the statistical peculiar velocity model, the TRGB data points support a value of $H_0=73$. Since these two were the principal sources of the Hubble tension, their removal or correction resolves the Hubble tension problem.

We also made comparisons between the predictions of the new model and the

Figure 21. The portion of the lunar recession due to the expansion of the universe.

parameter fits of the ΛCDM model and found that the new model prediction with $H_0 = 73$ matches the latter almost exactly in the redshift range $z \leq 1$ which is a validation of the new model. For larger redshifts, there are differences between the models but there do not exist sufficient data at present to make a judgment about which is closer to reality.

Acknowledgments

We wish to thank Ana Luisa Gonzales-Moran for sending us the HII data points we used in **Figure 6**.

Conflicts of Interest

The author declares no conflicts of interest regarding the publication of this paper.

References

[1] Botke, J.C. (2020) A Different Cosmology: Thoughts from Outside the Box. *Journal of High Energy Physics, Gravitation and Cosmology*, **6**, 473-566. https://doi.org/10.4236/jhepgc.2020.63037

[2] Hobson, M.P., *et al.* (2006) General Relativity, an Introduction for Physicists. Cambridge University Press, Cambridge, MA.

[3] Riess, A.G., *et al.* (1998) Observational Evidence from Supernovae for an Accelerating Universe and a Cosmological Constant. *Astrophysical Journal*, **116**, 1009-1038. https://doi.org/10.1086/300499

[4] Riess, A.G., *et al.* (2022) A Comprehensive Measurement of the Local Value of the Hubble Constant with 1 km s^{-1} Mpc^{-1} Uncertainty from the Hubble Space Telescope and the SH0ES Team. *The Astrophysical Journal Letters*, **934**, L7. https://doi.org/10.3847/2041-8213/ac5c5b

[5] Nielsen, J.T., Guffanti, A. and Sarkar, S. (2016) Marginal Evidence for Cosmic Acceleration from Type Ia Supernovae. *Scientific Reports*, **6**, Article No. 35596. https://doi.org/10.1038/srep35596

[6] Melnick, J., Moles, M., Terlevich, R. and Garcia-Pelayo, J.M. (1987) Giant HII Regions as Distance Indicators—I. Relations between Global Parameters for the Local Calibrators. *Monthly Notices of the Royal Astronomical Society*, **226**, 849-866. https://academic.oup.com/mnras/article/226/4/849/1003679

[7] Gonzales-Moran, A.L., *et al.* (2021) Independent Cosmological Constraints from High-Z HII Galaxies: New Results from VLT-KMOS Data. *Monthly Notices of the Royal Astronomical Society*, **505**, 1441-1457. https://academic.oup.com/mnras/article-abstract/505/1/1441/6276732?redirectedFrom=fulltext

[8] Pesce, D.W., *et al.* (2020) The Megamaser Cosmology Project. XIII. Combined Hubble Constant Constraints. *The Astrophysical Journal Letters*, **891**, L1. https://doi.org/10.3847/2041-8213/ab75f0

[9] Graziani, R., *et al.* (2018) The Peculiar Velocity Field up to $z \sim 0.05$ by Forward-Modeling Cosmicflows-3 Data. *Monthly Notices of the Royal Astronomical Society*, **488**, 5438-5451. https://academic.oup.com/mnras/article/488/4/5438/5289908

[10] The Extragalactic Distance Database (EDD) https://edd.ifa.hawaii.edu

[11] Freedman, W.L. (2021) Measurements of the Hubble Constant: Tensions in Perspective. *The Astrophysical Journal*, **919**, 1-22. https://doi.org/10.3847/1538-4357/ac0e95

[12] Botke, J.C. (2022) The Origin of Cosmic Structure, Part 4—Nucleosynthesis. *Journal of High Energy Physics, Gravitation and Cosmology*, **8**, 768-799. https://doi.org/10.4236/jhepgc.2022.83053

[13] Rivolo, A.R. (1985) The Two-Point Galaxy Correlation Function of the Local Supercluster. *The Astrophysical Journal*, **301**, 70-76. https://articles.adsabs.harvard.edu/full/1986ApJ...301...70R

[14] Bassett, B.A. and Hlozek, R. (2009) Baryon Acoustic Oscillations. https://arxiv.org/pdf/0910.5224.pdf

[15] Williams, J.G., Boggs, D.H. and Ratcli, J.T. (2016) Lunar Tidal Recession. 47*th Lunar and Planetary Science Conference*, The Woodlands, Texas, 2016, 1096-1100. https://www.hou.usra.edu/meetings/lpsc2016/pdf/1096.pdf

[16] Maeder, A.M. and Gueorguiev, V.G. (2021) On the Relation of the Lunar Recession and the Length-of-the-Day. *Astrophysics and Space Science*, **366**, Article No. 101. https://doi.org/10.1007/s10509-021-04004-7